Ships and Offshore Structures

ISSN: 1744-5302 (Print) 1754-212X (Online) Journal homepage: http://www.tandfonline.com/loi/tsos20

A higher-order nonlinear oscillator model for coupled cross-flow and in-line VIV of a circular cylinder

Zhuang Kang, Cheng Zhang & Rui Chang

To cite this article: Zhuang Kang, Cheng Zhang & Rui Chang (2018) A higher-order nonlinear oscillator model for coupled cross-flow and in-line VIV of a circular cylinder, Ships and Offshore Structures, 13:5, 488-503, DOI: 10.1080/17445302.2018.1426431

To link to this article: https://doi.org/10.1080/17445302.2018.1426431

SHIPS AND OFFSHORE STRUCTURES, 2018
VOL. 13, NO. 5, 488–503
https://doi.org/10.1080/17445302.2018.1426431

Taylor & Francis
Taylor & Francis Group

A higher-order nonlinear oscillator model for coupled cross-flow and in-line VIV of a circular cylinder

Zhuang Kang, Cheng Zhang and Rui Chang

Deepwater Engineering Research Centre, Harbin Engineering University, Harbin, China

ABSTRACT

In this paper, a higher-order nonlinear oscillator model has been proposed to predict the characteristics of the vortex-induced vibration (VIV) of a cylinder with two degrees of freedom. First, the vibration equations of the cylinder fixed by four symmetric springs were deduced based on the Lagrangian second kind of kinetic equation and the Taylor expansion formula of the binary function. Then, the fluctuating lift and drag were derived by using the discrete point vortex theory. Finally, the coupling model of the VIV was proposed by introducing the modified Van der Pol equation. On this basis, the VIV prediction of the cylinders with different mass ratios and damping ratios was carried out, and the results were compared with the experimental data to verify correctness and universality of the model. Besides, the sensitivity of the parameters in the model was analysed to investigate the predicting characteristics of the model systematically.

ARTICLE HISTORY
Received 28 July 2017
Accepted 5 January 2018

KEYWORDS
Vortex-induced vibration; oscillator model; nonlinear; higher-order

1. Introduction

Vortex-induced vibration (VIV) exists widely in many engineering fields, such as the risers in offshore oil and gas exploration, bridges, cables, antennas, etc. (Wanderley and Soares 2015). When the fluid with a certain velocity runs through the cylindrical structures, the phenomenon of periodic vortex shedding will occur. The continuous generation and shedding of the vortex will produce the fluctuating lift and drag, which will lead to the cross-flow and in-line VIV of the structures (Rahman et al. 2016; Gao et al. 2017). And the VIV is one of the important reasons for structural fatigue damage.

The research on the VIV of a cylinder is the basis of that of the cylindrical ocean structures. In recent years, a large number of scholars, such as Govardhan and Williamson (2000), Jauvtis and Williamson (2004), Prasanth and Mittal (2008), Guilmineau and Queutey (2004) and Nguyen and Nguyen (2016) have carried out many model tests or CFD numerical simulations to investigate the phenomena and induced mechanism of VIV. The research content of the two methods is abundant. But the cost of the model test is higher, and CFD numerical simulation is relatively complicated, especially in the case of high Reynolds number, the numerical simulation of the VIV is difficult to meet the actual needs of the engineering. Therefore, it is widely attractive to establish the relevant mathematical model and select the appropriate empirical parameters to predict the important characteristics of the VIV of structures quickly.

Bishop and Hassan (1964) first proposed a self-exciting and self-limiting Van der Pol equation to simulate the lift effect of fluid on the structure in VIVs. After that, Hartlen et al. (1970) improved the model proposed by Bishop and Hasson, where the structural vibration velocity was coupled with the Van der Pol equation. And the improved model is also the first proposed wake oscillator model. Based on their research, Griffin and Skop (1976), Facchinetti et al. (2004) and Farshidianfar and Zanganeh (2010) did some research on the wake oscillator model and acquired certain achievements, which also made the wake oscillator model become the most classical prediction model for the VIV of cylinders gradually. However, most of their researches have only considered the cross-flow vibration in VIV, and the in-line vibration which has the high-frequency characteristics and the coupling effect on cross-flow vibration cannot be ignored in many cases, especially for the structures with lower mass ratio, such as marine risers.

Srinil and Zanganeh (2012) employed two Duffing equations and two Van der Pol equations to simulate the VIV of the cylinder with two degrees of freedom. But in their mathematic model, the fluctuating lift and the fluctuating drag are disconnecting, so it is difficult to fully consider the coupling effect of the in-line and cross-flow vibration. Qin et al. (2012) deduced the fluid forces of the cylinder in VIV based on the method of discrete vortex, and then he proposed a model to predict relevant characteristics of the VIV with two-degree-of-freedom by combining the linear vibration equation of structure with the classical Van der Pol equation. However, the linearisation hypotheses in the prediction model for two-degree-of-freedom VIV are too much, which makes the accuracy of the predicting results still need to be improved.

CONTACT Cheng Zhang orangez@hrbeu.edu.cn

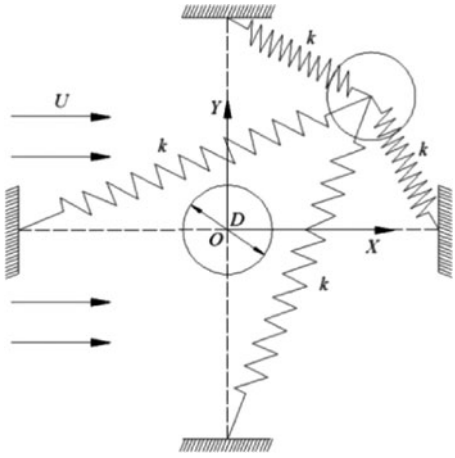

Figure 1. Schematic diagram of the vibrating model of a cylinder with two degrees of freedom.

In order to predict the amplitude response, frequency, motion trajectory and other important characteristics of the two-degree-of-freedom VIV of a cylinder qualitatively and quantitatively, the vibrating equations for the cylinder fixed by four symmetric springs have been deduced on the basis of Lagrangian second kind of kinetic equation, where the axial stretching nonlinearity and the coupling nonlinearity in the springs system are considered. So, the traditional linear vibrating equations of the structures are modified as the nonlinear equations to improve the predicting accuracy. Then, based on the Biot–Savart law and the Blasius' resultant forcing formula for the unsteady flow, the fluctuating fluid forces of the cylinder have been derived. And the mathematic relationship between the fluctuating lift and fluctuating drag has also been obtained from the mechanism of vortex-induced hydrodynamic force. Finally, a high-order Van der Pol equation with fifth-order aerodynamic damping term which can better simulate the hysteresis phenomenon and the super-upper branch of the amplitude in the VIV of the cylinder with low mass ratio has been introduced. On this basis, a higher-order nonlinear oscillator model is proposed to predict the amplitude and other characteristics of the VIV of the cylinder with two-degree-of-freedom, and then the model is verified and analysed for the cylinders with different mass ratios and damping ratios. The sensitivity of each parameter in the model is also analysed to study the forecasting characteristics of the model systematically.

2. Establishment of the higher-order nonlinear oscillator model

2.1. Nonlinear structural vibration equation

The VIV of the structure has strong nonlinear characteristics (Zhu and Gao 2017). When the cylinder is fixed by several springs, the system no longer meets the linear condition, especially for the VIV of the cylinder with double degrees of freedom. The vibration model for that is shown in Figure 1, and the coupling of the four springs makes the motion of the cylinder exhibits nonlinear characteristics.

For the vibration model in Figure 1, we define the stiffness coefficients of the four springs are all k, the original lengths are all a and the springs are in the original long state when the cylinder is in the central equilibrium position. For the system, the kinetic energy is given by

$$T = \frac{1}{2}m(\dot{X}^2 + \dot{Y}^2) \tag{1}$$

And the potential energy is described by

$$V = \frac{k}{2}\left(\sqrt{(a-X)^2+Y^2}-a\right)^2 + \frac{k}{2}\left(\sqrt{(a+X)^2+Y^2}-a\right)^2 + \frac{k}{2}\left(\sqrt{X^2+(a-Y)^2}-a\right)^2 + \frac{k}{2}\left(\sqrt{X^2+(a+Y)^2}-a\right)^2 \tag{2}$$

The Lagrange function of the system is expressed as

$$L = T - V = \frac{1}{2}m(\dot{X}^2+\dot{Y}^2) - \frac{k}{2}\left(\sqrt{(a-X)^2+Y^2}-a\right)^2 - \frac{k}{2}\left(\sqrt{(a+X)^2+Y^2}-a\right)^2 - \frac{k}{2}\left(\sqrt{X^2+(a-Y)^2}-a\right)^2 - \frac{k}{2}\left(\sqrt{X^2+(a+Y)^2}-a\right)^2 \tag{3}$$

And considering the generalised forces are the fluid force F_X and F_Y as well as the damping force $c\dot{X}$ and $c\dot{Y}$, the second kinds of Lagrange dynamic equation for the system can be expressed as

$$\frac{d}{dt}\left(\frac{\partial L}{\partial \dot{q}_j}\right) - \frac{\partial L}{\partial q_j} = F_{q_j} - c\dot{q}_j \tag{4}$$

where q_j is X or Y in the vibrating system. By solving formula (4), the equations of motion in X and Y directions can be derived as

$$m\ddot{X} + c\dot{X} + 4kX - \frac{ka(X-a)}{\sqrt{(X-a)^2+Y^2}} - \frac{ka(X+a)}{\sqrt{(X+a)^2+Y^2}} - \frac{kaX}{\sqrt{X^2+(Y-a)^2}} - \frac{kaX}{\sqrt{X^2+(Y+a)^2}} = F_X \tag{5a}$$

$$m\ddot{Y} + c\dot{Y} + 4kY - \frac{ka(Y-a)}{\sqrt{X^2+(Y-a)^2}} - \frac{ka(Y+a)}{\sqrt{X^2+(Y+a)^2}} - \frac{kaY}{\sqrt{(X-a)^2+Y^2}} - \frac{kaY}{\sqrt{(X+a)^2+Y^2}} = F_Y \tag{5b}$$

It can be found that Equations (5a) and (5b) are nonlinear coupling equations. And their nonlinearity is mainly reflected in the geometric nonlinearity of the springs. These equations are complicated and difficult to solve directly, so we need to simplify them. The nonlinear terms in above equations are expanded to the third order by using the Taylor expansion formula of the binary function shown in in the following equation:

$$f(X,Y) = f(X_0,Y_0) + \left[(X-X_0)\frac{\partial}{\partial X} + (Y-Y_0)\frac{\partial}{\partial Y}\right]f(X_0,Y_0) + \frac{1}{2!}\left[(X-X_0)\frac{\partial}{\partial X} + (Y-Y_0)\frac{\partial}{\partial Y}\right]^2 f(X_0,Y_0) + \cdots + \frac{1}{n!}\left[(X-X_0)\frac{\partial}{\partial X} + (Y-Y_0)\frac{\partial}{\partial Y}\right]^n f(X_0,Y_0) + R_n(3-53) \tag{6}$$

According to Equation (6), the $ka(X-a)/\sqrt{(X-a)^2+Y^2}$, $ka(X+a)/\sqrt{(X+a)^2+Y^2}$, $kaX/\sqrt{X^2+(Y-a)^2}$ and $kaX/\sqrt{X^2+(Y+a)^2}$ are expanded at $(0,0)$, respectively, and the items higher than the third order are omitted. Thus, the four nonlinear terms in Equation (5a) can be expressed as

$$\frac{(X-a)}{\sqrt{(X-a)^2+Y^2}} = -1+\frac{Y^2}{2a^2}+\frac{XY^2}{a^3} \tag{7a}$$

$$\frac{(X+a)}{\sqrt{(X+a)^2+Y^2}} = 1-\frac{Y^2}{2a^2}+\frac{XY^2}{a^3} \tag{7b}$$

$$\frac{X}{\sqrt{X^2+(Y-a)^2}} = \frac{X}{a}+\frac{XY}{a^2}-\frac{X^3}{2a^3}+\frac{XY^2}{a^3} \tag{7c}$$

$$\frac{X}{\sqrt{X^2+(Y+a)^2}} = \frac{X}{a}-\frac{XY}{a^2}-\frac{X^3}{2a^3}+\frac{XY^2}{a^3} \tag{7d}$$

The four nonlinear terms in Equation (5b) can be expanded similarly. Then, Equations (5a) and (5b) can be simplified to

$$m\ddot{X}+c\dot{X}+2kX-\frac{4kXY^2}{a^2}+\frac{kX^3}{a^2}=F_X \tag{8a}$$

$$m\ddot{Y}+c\dot{Y}+2kY-\frac{4kYX^2}{a^2}+\frac{kY^3}{a^2}=F_Y \tag{8b}$$

Meanwhile, the stiffness X and Y directions, the mass and the damping are, respectively, given by $k_x=k_y=2k$, $m=m_s+m_a$ and $c=c_s+c_f$ where m_s is the structural mass, m_a is the fluid added mass defined as $m_a=C_a\pi D^2\rho/4$ for a cylinder, c_s is the structural viscous damping coefficient, c_f is the added damping coefficient obtained by $c_f=\gamma\omega_{st}\rho D^2$ and $\gamma=\bar{C}_D/(4\pi St)$on the basis of Morrison formula with $\bar{C}_D$ the so-called average drag coefficient (Hartlen and Currie 1970). By introducing the geometric parameter $\eta=1/2a^2$, the modified nonlinear structural vibrations (Equations (8a) and (8b)) become

$$(m_s+m_a)\ddot{X}+(c_s+c_f)\dot{X}+k_x(X+\eta X^3-4\eta XY^2)=F_X \tag{9a}$$

$$(m_s+m_a)\ddot{Y}+(c_s+c_f)\dot{Y}+k_y(Y+\eta Y^3-4\eta YX^2)=F_Y \tag{9b}$$

We can find that the improved nonlinear structural vibration equations involve X^3, XY^2, Y^3 and YX^2, where X^3 and Y^3 mainly simulate the axial stretching nonlinearity in vibration, XY^2 and YX^2 mainly simulate the coupling nonlinearity of cross-flow and in-line vibration. Moreover, the improved equations have established the relation between the axial geometric nonlinear parameters and the coupled nonlinear parameters. So, the empirical parameters in the nonlinear terms are fewer, which can improve the accuracy of the calculation and reduce the computational complexity.

2.2. Derivation of the fluid forces

Due to the generation and shedding of the rear vortex of the cylinder, a lift F_L and drag F_D will be induced on the cylinder (Xu et al. 2017). We define a layer of area close to the surface of the cylinder as near-wall control field and the area outside the near-wall control field as wake vortex field.

By superimposing the N point vortices composed of m control vortices in the near-wall field and n stable vortices in the wake vortex field and the uniform flow, we can obtain the flow field complex potential $W(z)$. Based on the Blasius' resultant forcing formula for the unsteady flow, the fluid forces acting on the cylinder are given by

$$F_D-iF_L=\oint_c i(\rho\frac{\partial W}{\partial t}+\frac{\rho}{2}\frac{dW}{dz}\frac{d\bar{W}}{d\bar{z}})d\bar{z} \tag{10}$$

By using the formula of $\bar{z}_k z_k^*=R^2$, Equation (11) can be deduced to

$$F_D=\frac{\rho D}{4}\sum_{k=1}^{m}\frac{\partial\Gamma_k}{\partial t}\frac{y_k}{{x_k}^2+{y_k}^2}+\rho\sum_{k=1}^{N}\Gamma_k \times\left[-\upsilon_k-\frac{u_k}{4}\frac{2x_ky_k}{({x_k}^2+{y_k}^2)^2}+\frac{\upsilon_k}{4}\frac{{x_k}^2-{y_k}^2}{({x_k}^2+{y_k}^2)^2}\right] \tag{11a}$$

$$F_L=-\frac{\rho D}{4}\sum_{k=1}^{m}\frac{\partial\Gamma_k}{\partial t}\frac{x_k}{{x_k}^2+{y_k}^2}+\rho\sum_{k=1}^{N}\Gamma_k \times\left[u_k+\frac{u_k}{4}\frac{{x_k}^2-{y_k}^2}{({x_k}^2+{y_k}^2)^2}+\frac{\upsilon_k}{4}\frac{2x_ky_k}{({x_k}^2+{y_k}^2)^2}\right] \tag{11b}$$

where u_k and υ_k are the induced velocities at the position of the kth point vortex.

The parts in the square brackets of the above equations are defined as f_{D1} and f_{L1}, respectively. In the wake vortex field, we assume the point vortex moves along the downstream and $x_ky_k/({x_k}^2+{y_k}^2)^2$ and $({x_k}^2-{y_k}^2)/({x_k}^2+{y_k}^2)^2$ tend to 0 in the far wake vortex field. So, f_{D1} and f_{L1} can be expressed approximately as

$$f_{D1}=0 \tag{12a}$$

$$f_{L1}=\rho U\sum_{k=m+1}^{N}\Gamma_k=\rho U\Gamma_n(t)=\rho\Gamma U\cos(2\pi\omega_{st}t) \tag{12b}$$

where ω_{st} is the vortex shedding frequency and Γ is the peak of total vorticity.

We denote the first term of the right part of Equations (12a) and (12b) as f_{D2} and f_{L2} which are shown in Equation (13):

$$f_{D2}=\frac{\rho D}{4}\sum_{k=1}^{m}\frac{\partial\Gamma_k}{\partial t}\frac{y_k}{{x_k}^2+{y_k}^2}\approx\rho D\sum_{k=1}^{m}\frac{\partial\Gamma_k}{\partial t}y_k=\rho D\frac{d\Gamma_C}{dt}y_C \tag{13a}$$

$$f_{L2}=-\frac{\rho D}{4}\sum_{k=1}^{m}\frac{\partial\Gamma_k}{\partial t}\frac{x_k}{{x_k}^2+{y_k}^2}\approx-\rho D\sum_{k=1}^{m}\frac{\partial\Gamma_k}{\partial t}x_k =-\rho D\frac{d\Gamma_C}{dt}x_C \tag{13b}$$

where x_C and y_C are the dimensionless positions of the equivalent vortex. And due to y_C vibrates at the positive and negative axis of the y-axis and x_C has a slight change at the positive axis of the x-axis, only the role of y_C is taken into account.

Based on the principle of the generation and dissipation of vortex, the change of vorticity of the equivalent vortex is opposite to that of the vortex in wake vortex field. Thus equivalent vortex Γ_C can be described by

$$\Gamma_C = -\Gamma \cos(2\pi\omega_{st}t) \tag{14}$$

The position of the positive point vortex and that of the negative point vortex in the near-wall field will alternately transform. And we can also use the cosine function to approximate this process. But considering the specific value of the amplitude is unknown, it is necessary to introduce an empirical parameter α determined by the experiment. So, y_C can be given by

$$y_C = \alpha\frac{\Gamma}{UD}\cos(2\pi\omega_{st}t) \tag{15}$$

Then, f_{D2} and f_{L2} are derived as

$$f_{D2} = \rho D\,[2\pi\omega_{st}\Gamma\sin(2\pi\omega_{st}t)]\left[\alpha\frac{\Gamma}{UD}\cos(2\pi\omega_{st}t)\right] \tag{16a}$$

$$f_{L2} = 0 \tag{16b}$$

F_D and F_L can be obtained by adding f_{D1} and f_{D2} as well as f_{L1} and f_{L2}. We introduce a dimensionless wake variable $q = 2C_L/C_{L0}$ where C_{L0} is the reference lift coefficient. And then considering $F_L = \rho DU^2C_L/2$, we can obtain $4\Gamma\cos(2\pi\omega_{st}t) = UDC_{L0}q$. Thus, the cross-flow and in-line fluid forces F_X and F_Y are described by

$$F_X = F_D = -\frac{1}{16}\rho D^2{C_{L0}}^2\alpha Uq\dot{q} \tag{17a}$$

$$F_Y = F_L = \frac{1}{4}\rho DC_{L0}U^2q \tag{17b}$$

2.3. Higher-order modification of the Van der Pol equation

The classical wake oscillator model usually simulates the motion of the fluid oscillator by using the Van der Pol equation. Facchinetti et al. (2002) and (2004), in their study, argued that the excitation term of the Van der Pol equation was related to the acceleration of the cross-flow vibration. Researchers such as Farshidianfar and Zanganeh (2010) and Dolatabadi et al. (2011) found that although the classical wake oscillator model was well able to predict the VIV response of the cylinder with high mass ratio, it often underestimated the amplitude results under the condition of low mass ratio. So, it is necessary to modify it.

Based on the higher-order Van der Pol equation proposed by Landl (1975) and the research of Farshidianfar on single-degree-of-freedom VIV, the classical wake oscillator model is modified by high order in this paper. Landl's higher-order model includes a Van der Pol damping term and a fifth-order aerodynamic damping term, and specific formula is given by

$$\ddot{C}_L + (\alpha' - \beta'{C_L}^2 + \lambda'{C_L}^4)\dot{C}_L + \Omega_r C_L = b\dot{y} \tag{18}$$

where Ω_r is the structural vibration frequency, α', β', λ' and b are empirical parameters and need to be selected according to different specific problems. By transforming Equation (18) into the form of the Van der Pol equation and introducing parameters $\alpha' = -\varepsilon$, $\beta'/\varepsilon = -\beta$ and $\lambda'/\varepsilon = \lambda$, we can obtain

$$\ddot{q} + \varepsilon\omega_{st}(\beta q^2 - 1 + \lambda q^4)\dot{q} + {\omega_{st}}^2 q = F \tag{19}$$

where ω_{st} is the Strouhal frequency with $\omega_{st} = 2\pi StV/D$. In the research of Farshidianfar, the displacement, velocity and acceleration of the structure are substituted into F to analyse the model, and the results of the acceleration were found to be best. So, the $F = H\ddot{Y}$ is taken as the coupling term in Equation (19), where H is the empirical parameter confirmed by the experimental data.

It can be found that the higher-order equation is connected with the classical Van der Pol equation. When $\beta = 1$ and $\lambda = 0$, the higher-order equation is equal to the classical Van der Pol equation. By adjusting the value of β and λ, the higher-order equation can increase the amplitude of vibration properly. So, it can effectively overcome some disadvantages of classical Van der Pol equation, which is difficult to accurately simulate the high amplitude response under the condition of low mass ratio.

To verify the enlargement effect of β and λ on vibration amplitude, the higher-order and classical Van der Pol equations are calculated by combining cross-flow vibration equation investigated by Facchinetti et al. (2004) and Farshidianfar and Zanganeh (2010), which is shown in the following equation:

$$\ddot{y} + \left(2\xi\delta + \frac{\gamma}{\mu}\right)\dot{y} + \delta^2 y = S, \quad S{=}Mq{=}\frac{C_{L0}}{2}\frac{1}{8\pi^2St^2\mu}q \tag{20}$$

Using a harmonic linearisation method for Equations (19) and (20) and assuming $y(t) = y_0\cos(\omega t)$ and $q(t) = q_0\cos(\omega t - \phi)$, elementary algebra yields the amplitude y_0 and q_0

$$\frac{y_0}{q_0} = \frac{M}{\sqrt{(\delta^2-\omega^2)^2 + \left(2\xi\delta + \frac{\gamma}{\mu}\right)^2\omega^2}} \tag{21a}$$

$$q_0 = 2\sqrt{\frac{-\beta + \sqrt{\beta^2 + 8\lambda\left(1 + \frac{AM}{\varepsilon}\frac{C}{\left(\delta^2-\omega^2\right)^2 + (2\xi\delta+\gamma/\mu)^2\omega^2}\right)}}{4\lambda}} \tag{21b}$$

$$\omega^6 - \left[1 + 2\delta^2 - \left(2\xi\delta + \frac{\gamma}{\mu}\right)^2\right]\omega^4 - \left[-2\delta^2 + \left(2\xi\delta + \frac{\gamma}{\mu}\right)^2 - \delta^4\right]\omega^2 - \delta^2 + G = 0 \tag{21c}$$

where $C = (2\xi\delta + \gamma/\mu)\omega^2$, $G = hM(\omega^2 - \delta^2)\omega^2$, parameters ε, h, β and λ are selected as 0.3, 12, 0.25 and 0.008. The calculated results about amplitude y_0 and q_0 using higher-order and classical Van der Pol equations are illustrated in Figure 2.

It can be observed that the value of q_0 and y_0 increases at all reduced velocities while the lock-in and hysteresis intervals are almost unchanged after introducing the parameters β and λ, which indicates that the higher-order Van der Pol equation can be applied in the prediction for the higher amplitude VIV that usually occurs in the marine and ocean engineering field.

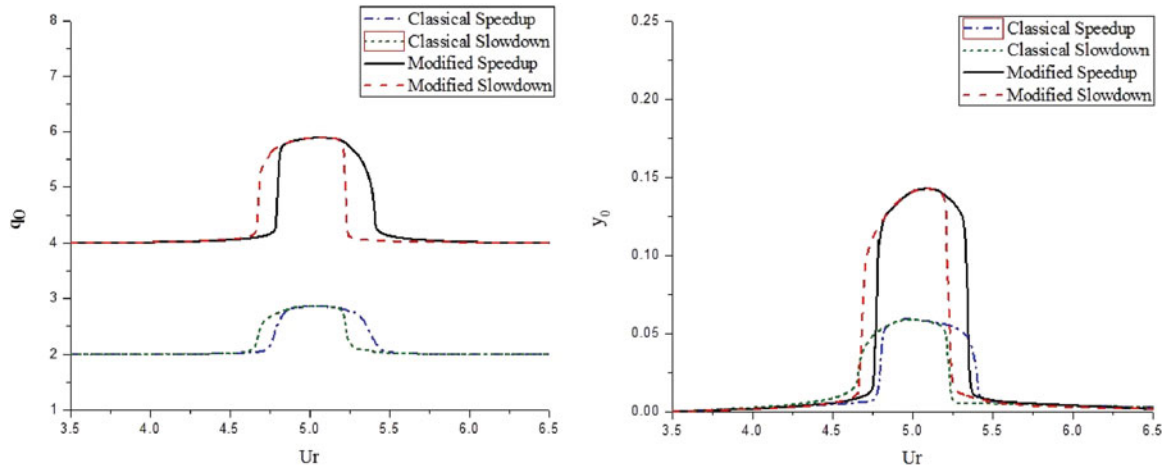

Figure 2. Comparison of the amplitude results about higher-order and classical Van der Pol equations; (a) amplitude of the wake oscillator q_0; (b) amplitude of the structure oscillator y_0. (This figure is available in colour online.)

2.4. Coupled nonlinear oscillator equation

By combining the structural vibration equation and the fluid oscillator equation, we can obtain the coupled equations of the VIV of cylinders. Meanwhile, the dimensionless process is carried out, where $\tau = \omega_{st}t$, $x = X/D$ and $y = Y/D$ as well as the empirical parameter $\alpha = C_{D0}/(2\pi St{C_{L0}}^2)$ are introduced. And the coupled nonlinear oscillator equations are expressed as

$$\frac{d^2x}{d\tau^2} + \left(2\xi\delta + \frac{\gamma}{\mu}\right)\frac{dx}{d\tau} + \delta^2(x + \eta x^3 - 4\eta x y^2) = -\frac{C_{D0}q\dot{q}}{32\pi^2 St^2\mu} \tag{22a}$$

$$\frac{d^2y}{d\tau^2} + \left(2\xi\delta + \frac{\gamma}{\mu}\right)\frac{dy}{d\tau} + \delta^2(y + \eta y^3 - 4\eta y x^2) = \frac{C_{L0}q}{16\pi^2 St^2\mu} \tag{22b}$$

$$\ddot{q} + \varepsilon(\beta q^2 - 1 + \lambda q^4)\dot{q} + q = h\frac{d^2y}{d\tau^2} \tag{22c}$$

where $\xi = c_s/(2m_s\omega_n)$ is the structural damping ratio, ω_n is the natural vibrating frequency of the cylinder; μ is a dimensionless mass ratio parameter with $\mu = (m_s + m_a)/\rho D^2$; $\delta = \omega_n/\omega_{st}$ is the frequency ratio; γ is the damping parameter of fluid, being selected as 0.5 based on the research of Ogink and Metrikine (2010), with $\gamma = C_d/(4\pi St)$; η is the geometric nonlinear parameter, being taken as 0.2 by fitting with the experimental results (Jauvtis and Williamson 2004; Stappenbelt et al. 2007; Blevins and Coughran 2009); h is a dimensionless coupling parameter selected as 12 on the basis of the research of Facchinetti et al. (2004); ε is the damping parameter of Van der Pol equation related to the mass ratio of cylinder, being determined by the fitting curve (Jauvtis and Williamson 2004; Stappenbelt et al. 2007), as shown in Figure 3; β and λ are the nonlinear parameters of fluid oscillator. In addition, C_{L0} and C_{D0} are the referenced lift and drag coefficient, respectively which are taken as 0.3 and 0.2 based on the researches of Blevins and Coughran (2009) and Pantazopoulos (1994).

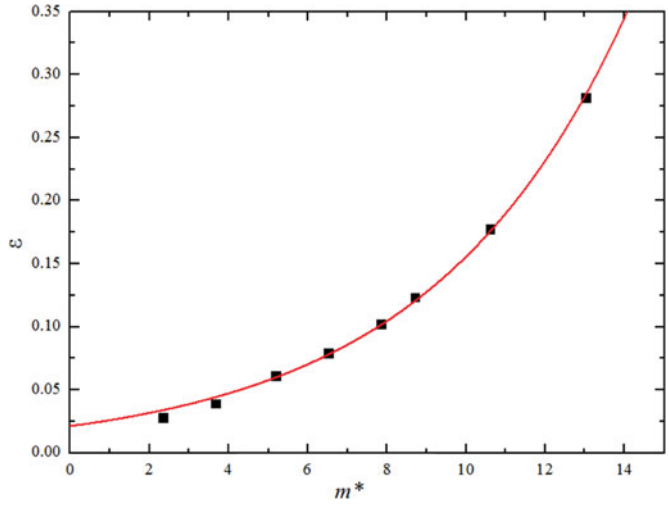

Figure 3. Fitting curve of ε for different mass ratios of cylinders. (This figure is available in colour online.)

The parameters β and λ are determined by referring to the solving method for nonlinear equations proposed by Nayfeh (1979). Without external disturbances, the higher-order Van der Pol equation is given by

$$\ddot{q} + q = \varepsilon(-\beta q^2 + 1 - \lambda q^4)\dot{q} \tag{23}$$

The solution of the equation can be divided into linear part and nonlinear part. By ignoring the high-order nonlinear part, we can get

$$q(t, \varepsilon) = u(t) + \varepsilon v(t) + \cdots \tag{24}$$

Substituting Equation (24) into Equation (23), we can solve the linear and nonlinear parts separately. And these parts are described by

$$\ddot{u} + u = 0, \quad \ddot{v} + v = \ddot{u} - \frac{\beta}{3}\dot{u}^3 + \frac{\lambda}{5}\dot{u}^5 \tag{25}$$

Table 1. parameters of the cylinder.

D	$m^*\xi$	m^*	ξ	f_N	f_{Nx}/f_{Ny}
3.81cm	0.013	2.6	0.005	0.4 Hz	1

After the algebraic computation process, the solutions are given by

$$u = q_0 \cos \omega t \tag{26a}$$

$$v = \frac{1}{2}\left(1 - \frac{\beta}{4}{q_0}^2 + \frac{\lambda}{8}{q_0}^4\right) q_0 \cos \omega t + \frac{1}{8}\left(\frac{\beta}{12} - \frac{\lambda}{16}{q_0}^2\right){q_0}^3 \times \sin 3\omega t + \frac{\lambda}{1920}{q_0}^5 \sin 5\omega t \tag{26b}$$

When $t = 0$, we can obtain $1 - \beta/4{q_0}^2 + \lambda/8{q_0}^4 = 0$. And then q_0 is solved as

$$q_0 = \sqrt{-\frac{\beta}{\lambda} + \left(\left(\frac{\beta}{\lambda}\right)^2 + \frac{8}{\lambda}\right)^{0.5}} \tag{27}$$

It can be found that there are two independent variables in the above formula, namely β and λ. By setting the value of β from small to large, a series of formulas of q_0 changing with λ can be obtained. We can reasonably adjust the values of β and λ to change q_0, which will achieve the purpose of changing the vibration amplitudes of fluid oscillator and structural oscillator. For the model of this paper, β and λ are selected as 0.25 and 0.008, respectively by fitting with the experimental data, and the effects of the two parameters will be investigated in Section 4.3.

3. Verification and analysis of the model

3.1. Verification of the example of a cylinder

The experimental data of the example are derived from the model test of the two-degree-of-freedom VIV of a cylinder conducted by Jauvtis and Williamson (2004). The relevant parameters of the cylinder are shown in Table 1.

It should be noted that the mass ratio in Willamson's paper is defined as $m^*{=}m_s/m_\rho{=}\ 4m_s/\pi\rho D^2$, where m_s is the structure mass, m_ρ is the displaced fluid mass, for two-dimensional simulation, the length of the cylinder can be selected as 1. We can see the definition of mass ratio m^* is different with the dimensionless mass ratio parameter $\mu = \frac{m_s+m_a}{\rho D^2}{=}\frac{m^*\times\frac{\pi\rho D^2}{4}+C_M\times\frac{\pi\rho D^2}{4}}{\rho D^2} = \frac{\pi}{4}(m^*+C_M)$ introduced in Section 2.4, where C_M is the added mass coefficient and usually taken as 1 for a circular cylinder (Facchinetti et al. 2004). Then, μ can be written as $\mu = \frac{\pi}{4}(m^*{+}1)$, which describes the relationship of μ and m^*.

The higher-order nonlinear oscillator model is solved by using fourth-order Ronge–Kutta method, then the dimensionless amplitude and motion trajectory of the cylinder under different reduced velocity are obtained, and the dimensionless frequency is acquired by Fourier transform.

Besides the testing results of Jauvtis and Williamson, the results of the same circular cylinder calculated by the existing VIV analysis software Shear 7, where the classical wake oscillator model is adopted, are also presented. And the relevant results calculated by the two models are compared with the experimental results, as shown in Figures 4–6. It should be noted that since the Shear 7 can only consider the cross-flow vibration of the cylinder, just the representative cross-flow dimensionless amplitude of classical model is given.

By analysing the cross-flow dimensionless amplitude results of the new model in Figure 4(a), it can be found that when $U_r >$ 4, the cross-flow VIV of the cylinder gradually enters the resonance state, and its amplitude increases obviously. When $U_r > 8$, the vibration gradually starts to get out of resonance stage and the amplitude suddenly decreases to a smaller value, which is consistent with Williamson's test results in general trend. And the calculated results of the most important 'upper branch' and 'super upper branch' of the amplitude response are in good agreement with the experimental results. In addition, the calculated maximum amplitude is about 1.5D, which is very close to the experimental results. However, we can also find the new model does not accurately simulate the 'lower branch' of the amplitude mainly because the coupling parameter ε is chosen as a constant only related to the mass ratio. And the shape of the 'lower branch' may be adjusted by associating ε with the reduced

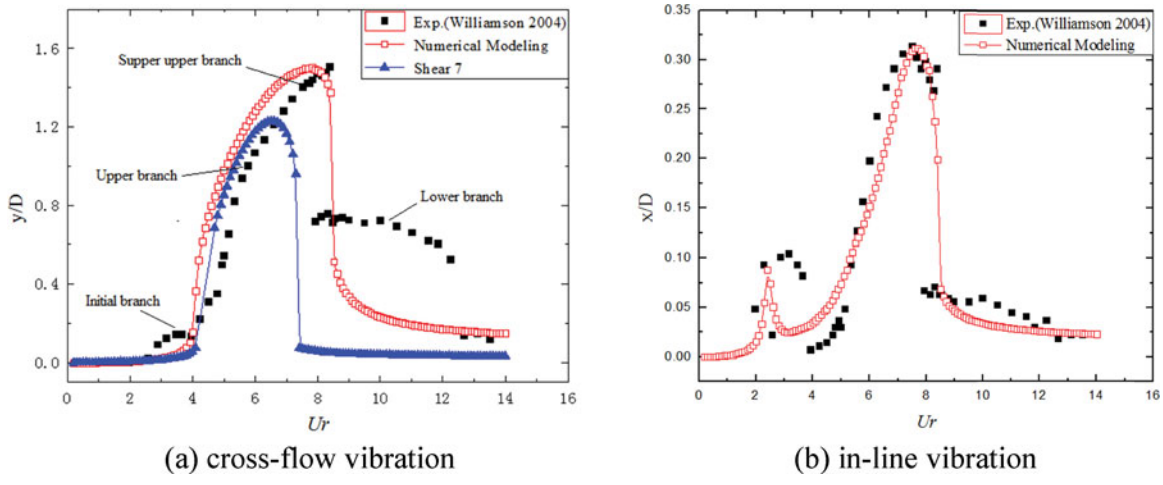

Figure 4. Comparison of the amplitude response of cylindrical vibration; (a) cross-flow vibration; (b) in-line vibration. (This figure is available in colour online.)

velocity, which can be further studied in the future. By contrast, although the 'upper branch' of the amplitude curve is predicted by the classical model in Shear 7, the most important 'super upper branch' is absent under the condition of low mass ratio, and the lock-in range is much smaller than experimental value. This is due to the classic wake oscillator model in Shear 7 ignores the coupling effect of in-line vibration on cross-flow vibration, and its empirical parameter is obtained from the single-degree-of-freedom model test, which has limited effect in the case of high mass ratio but leads to large errors under the condition of low mass ratio. Therefore, in engineering project, the safety factor is often larger when the Shear 7 software is used to analyse the VIV of the cylindrical structures, such as risers.

For the in-line dimensionless amplitude results in Figure 4(b), we can find a significant resonance appears at $U_r = 2.5$. And then its amplitude decreases rapidly, following which a larger increase of the in-line amplitude occurs on account of the coupling effect of cross-flow vibration on in-line vibration. When $U_r > 8$, the in-line amplitude decreases markedly since the cross-flow vibration is getting out of the resonance state and the coupling effect is relatively weak. The compared results show that the trend of in-line amplitude and the maximum value in calculation are in good agreement with the experimental results. And combined with the reasonable prediction of the amplitude response for cross-flow vibration, it is shown that the nonlinear oscillator model proposed in this paper can qualitatively and quantitatively predict the amplitude characteristics of the cylindrical two-degree-of-freedom VIV.

The calculated and experimental results of dimensionless frequency of cross-flow vibration are illustrated in Figure 5. It can be found that the calculated results occur the lock-in phenomenon when Ur is between about 4 and 9, and the results under other reduced velocities satisfy Strouhal relationship, which is basically consistent with the experimental data and the related theoretical studies. However, since the mathematical model fails to accurately simulate the 'lower branch' of cross-flow vibration in Wiiliamson's test, the frequency results have a certain difference with experimental data when Ur is larger. In general, the mathematical model can qualitatively reflect the frequency characteristics of the cylindrical VIV.

The calculated motion trajectories of the cylinder under different reduced velocity are shown in Figure 6. When the flow velocity is lower, the in-line amplitude is larger than the cross-flow amplitude, and the motion trajectory is flat or standard '8' shape, but its overall motion is relatively small. With the increase

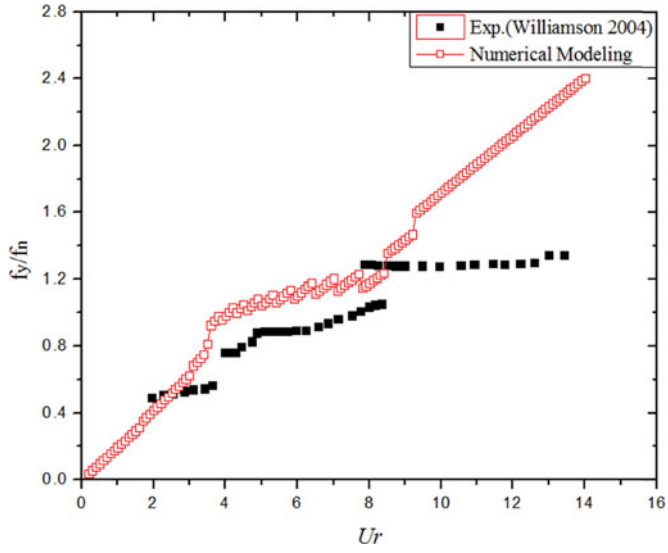

Figure 5. Comparison of the cross-flow dimensionless frequency of cylindrical vibration. (This figure is available in colour online.)

of the flow velocity, the cross-flow vibration gradually enters the resonance state and the amplitude increases significantly. At this time, the trajectory appears as the elongated '8' shape and gradually shows a tendency to tilt to the right side. And the trajectory is close to the crescent shape when Ur is near 8–9. And then, with the continuous increase of the flow velocity, both the in-line and the cross-flow amplitudes significantly decrease, and the motion trajectory becomes a narrow and thin '8' shape. The variation of these trajectories is basically consistent with the results of the current VIV studies.

In general, the higher-order nonlinear oscillator model proposed in this paper is able to simulate the amplitude, frequency and trajectory characteristics of two-degree-of-freedom VIV of the cylinder with relatively higher accuracy, which can provide a reference for research on quick prediction for the VIV characteristics of structures.

3.2. Influence of the mass ratio

The mass ratio is an important factor affecting the VIV characteristics of the cylinders. In this section, based on the model test of two-degree-of-freedom VIV of the cylinders carried out by Stappenbelt et al. (2007), the mass ratios are selected as 2.36, 3.68, 5.19, 6.54, 7.91 and 8.76, respectively and the damping ratio is chosen as 0.006. The values of ε at different mass ratios are

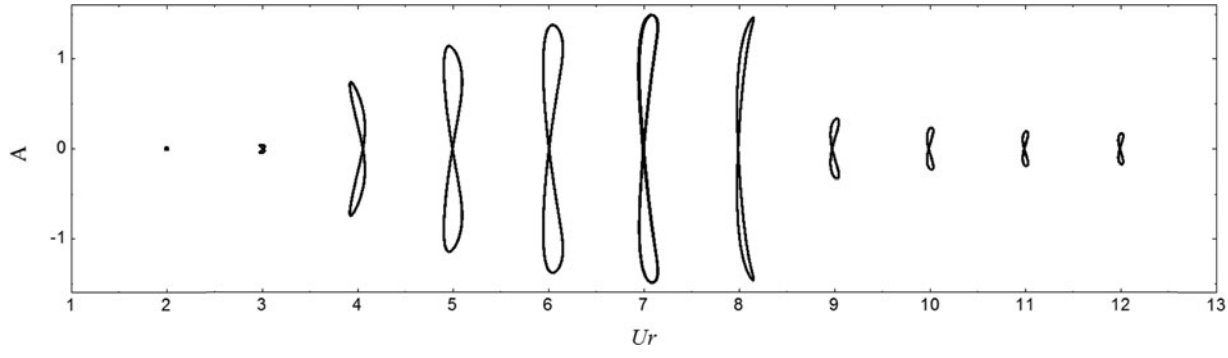

Figure 6. The motion trajectories of the two-degree-of-freedom VIV of the cylinder.

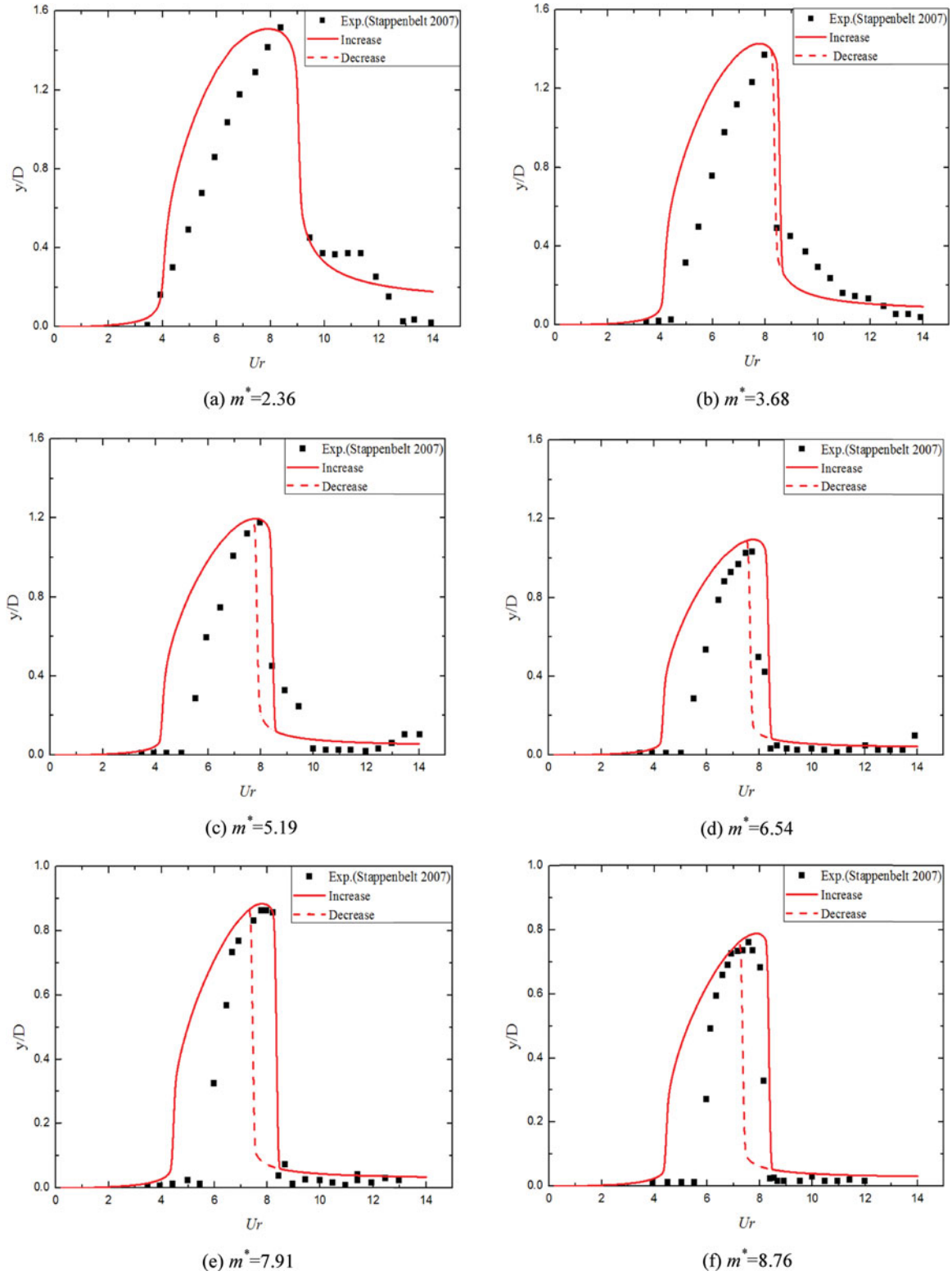

Figure 7. Comparison of the cross-flow amplitude of the cylinders with different mass ratios; (a) $m^* = 2.36$; (b) $m^* = 3.68$; (c) $m^* = 5.19$; (d) $m^* = 6.54$; (e) $m^* = 7.91$; (f) $m^* = 8.76$.

selected by using the curve in Figure 3 shown in Section 2.4. And then the predictions for the VIV of the cylinders with different mass ratios are conducted.

Figure 7 shows the calculated results and Stappenbelt's experimental results about the cross-flow amplitude of the cylinders with different mass ratios. After comparison, we can find the two kinds of results can be consistent in the trend under different mass ratio conditions, and the calculated maximum amplitude is in agreement with the experimental value. In addition, it can be found that as the mass ratio increases, the maximum amplitude of the cross-flow vibration and the lock-in range is decreasing, but the hysteresis interval predicted by the oscillator

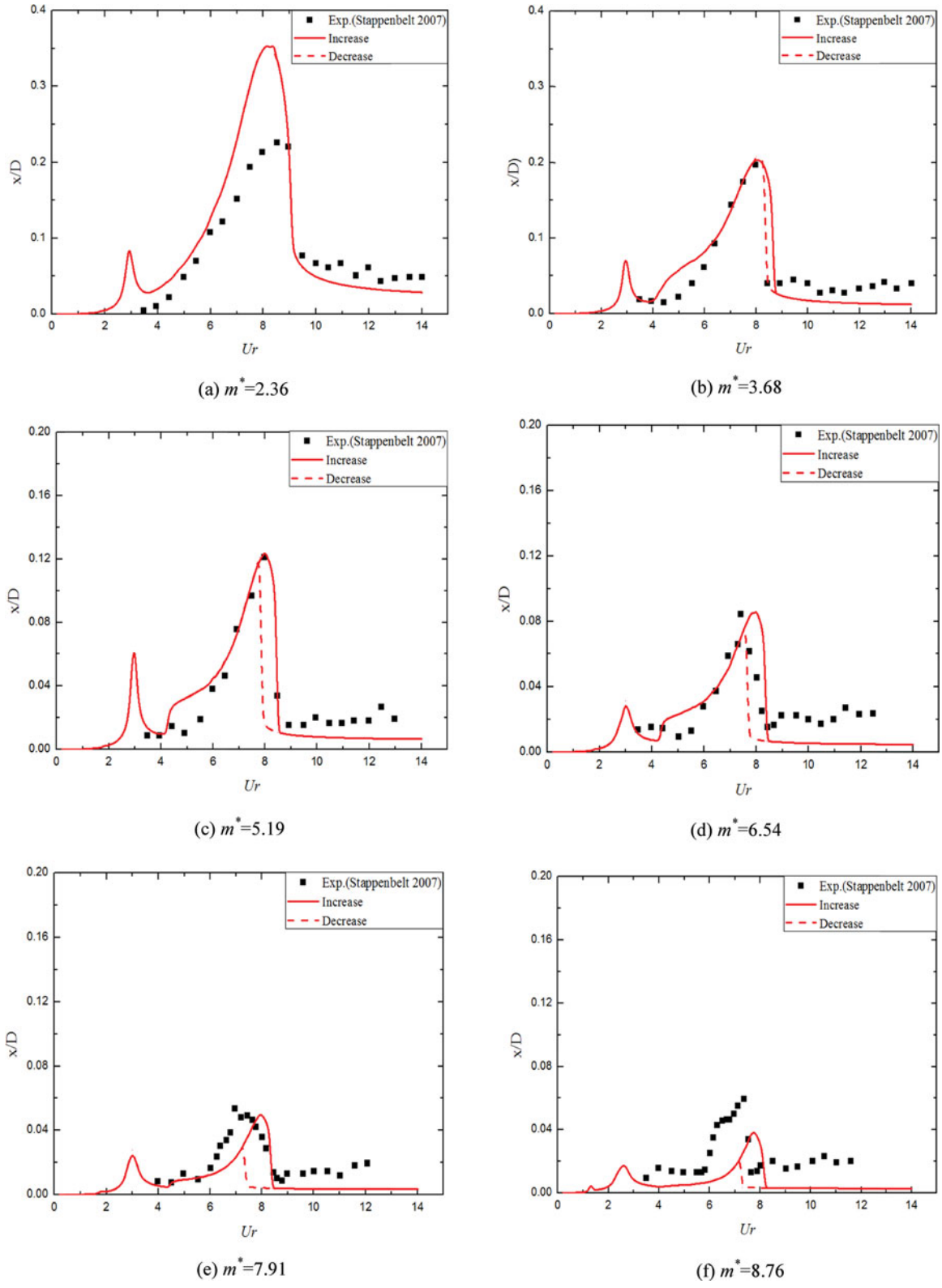

Figure 8. Comparison of the in-line amplitude of the cylinders with different mass ratios; (a) $m^* = 2.36$; (b) $m^* = 3.68$; (c) $m^* = 5.19$; (d) $m^* = 6.54$; (e) $m^* = 7.91$; (f) $m^* = 8.76$. (This figure is available in colour online.)

model is becoming larger. This is because the coupling parameter ε will increase with the mass ratio, which will enhance the nonlinearity of the model to further make the hysteresis interval larger.

By comparing and analysing the in-line amplitude curves in Figure 8, it is found that the calculated results are in good agreement with the experimental results in the trend, and the calculated maximum amplitude is basically consistent with the

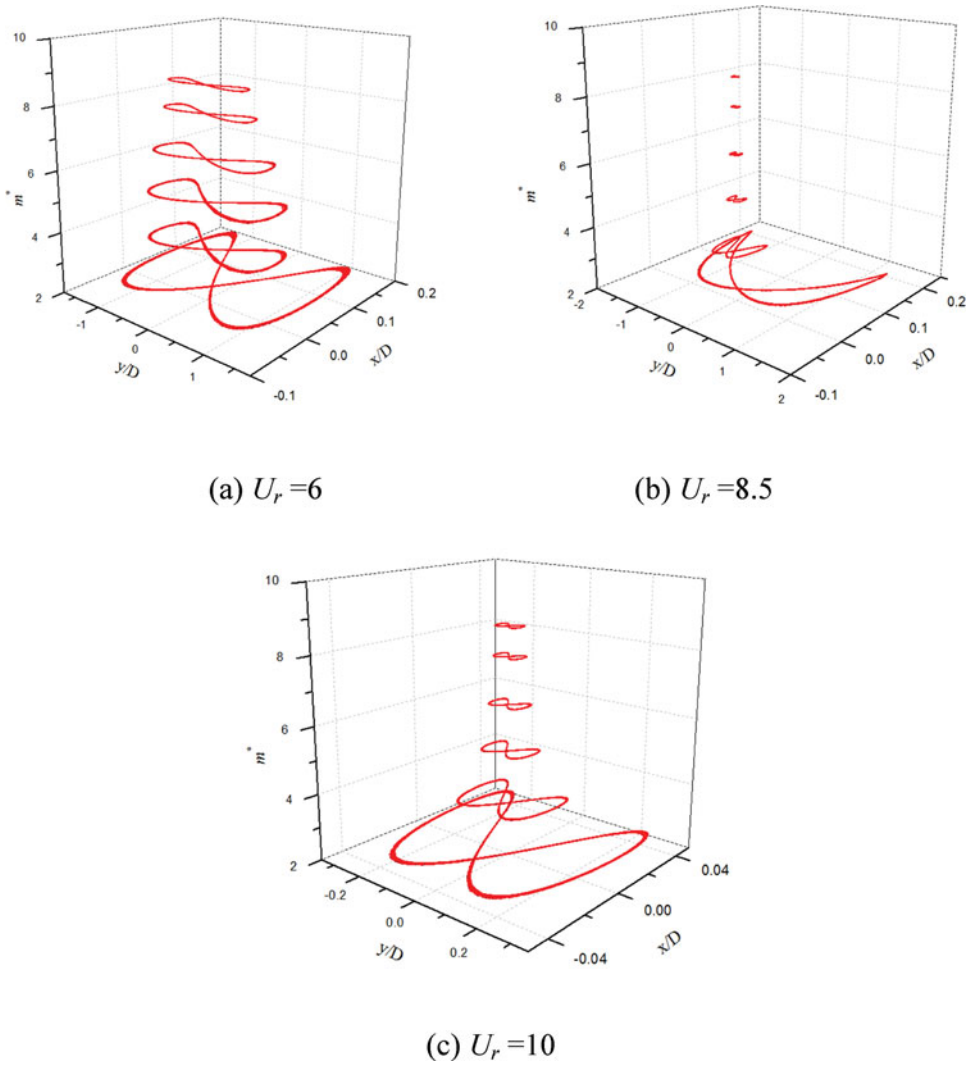

Figure 9. Comparison of the motion trajectories of the cylinders with different mass ratios; (a) $U_r = 6$; (b) $U_r = 8.5$; (c) $U_r = 10$. (This figure is available in colour online.)

experimental value. However, when the mass ratio is 2.36, the in-line maximum amplitude of the cylinder is overestimate. This is because the calculating formula of ε is the exponential form related to mass ratio, and the value of ε is insensitive when the mass ratio is very low, which results in a certain error. In addition, with the increase of the mass ratio, the coupling effect of the cross-flow vibration on in-line vibration is weakening, which leads to the decrease of its second peak. And similar to the cross-flow vibration, the in-line hysteresis interval also increases with the mass ratio.

In order to analyse the effect of mass ratio on the motion trajectory of the cylinder near the amplitude branch mutation, the trajectory curves with $Ur = 6$, 8.5 and 10 under different mass ratio conditions are given in Figure 9. It can be found that the '8' shape of the trajectory becomes thinner with the increase of mass ratio at $Ur = 6$, which is because the coupling effect of cross-flow vibration on in-line vibration decreases with the increase of mass ratio and the in-line amplitude becomes smaller. At $Ur = 8.5$, the trajectory appears as the crescent shape under the lower mass ratio condition. And with the increase of the mass ratio, the size of trajectory decreases greatly, and the crescent shape is not exhibited because the increase of mass ratio causes the reduction of lock-in range, which has contributed to the detachment from the lock-in region at $Ur = 8.5$. When $Ur = 10$, the trajectories become the '8' shape again under all mass ratio conditions, and the higher the mass ratio, the smaller the '8' shape.

3.3. Influence of the damping ratio

The damping ratio is another important parameter affecting the characteristics of VIV. By referring to the results of the model test for two-degree-of-freedom VIV of the cylinders conducted by Blevins and Coughran (2009) in 2009, we set the mass ratio of the cylinders as 5.4 and the damping ratio as 0.002, 0.02, 0.05, 0.1, 0.2 and 0.4, respectively, and then predict the characteristics of the VIV of the cylinders.

Figure 10 shows the cross-flow amplitude curves with different damping ratios. It can be found that the curve trend and the maximum value of the calculated results are in basic agreement with the experimental results. With the increase of damping ratio, the amplitude of cross-flow vibration is significantly reduced, and the hysteresis is no longer obvious, but the size of the locking range has little change.

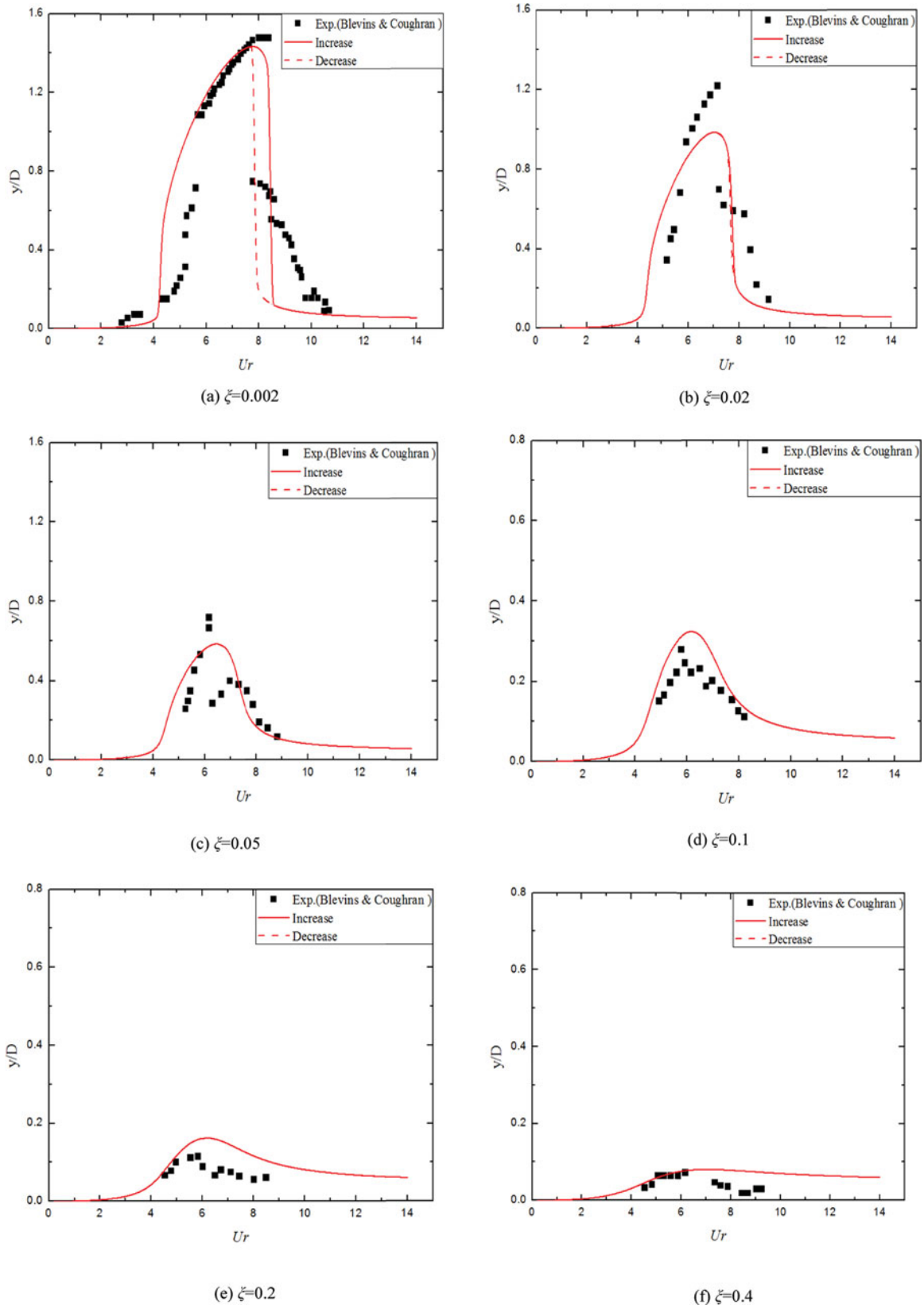

Figure 10. Comparison of the cross-flow amplitude of the cylinders with different damping ratios; (a) $\xi = 0.002$; (b) $\xi = 0.02$; (c) $\xi = 0.05$; (d) $\xi = 0.1$; (e) $\xi = 0.2$; (f) $\xi = 0.4$. (This figure is available in colour online.)

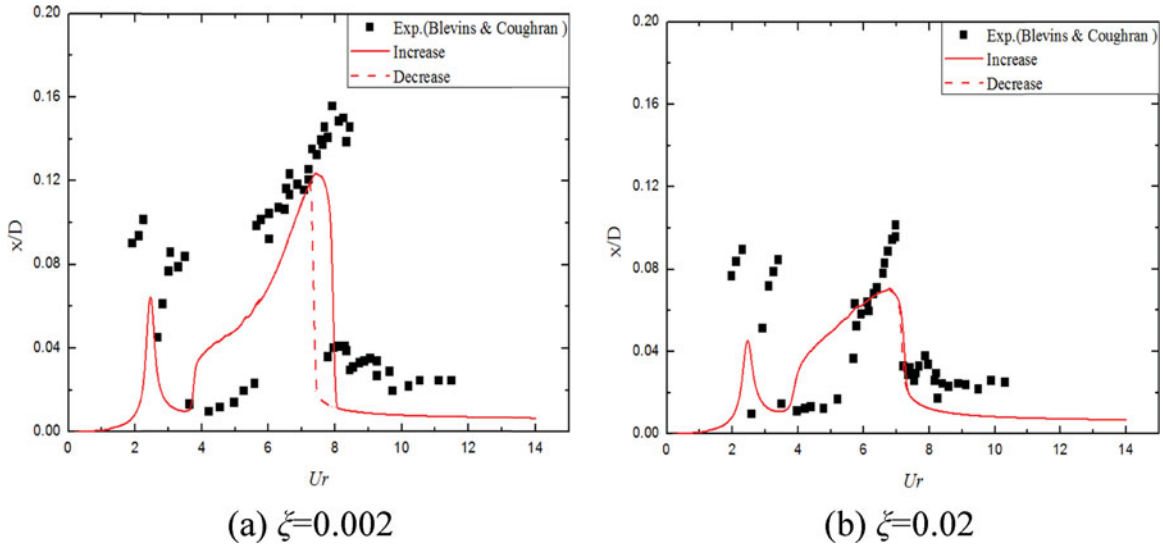

Figure 11. Comparison of the in-line amplitude of the cylinders with different damping ratios; (a) $\xi = 0.002$; (b) $\xi = 0.02$. (This figure is available in colour online.)

Figure 11 illustrates the in-line amplitude curves of the cylinders with different damping ratios. Since the in-line amplitude under the high damping ratio conditions is very small, we have only given the comparison results about the damping ratios 0.002 and 0.02. After comparison, we can find that the calculated results are consistent with the experimental results in the trend, but the calculated maximum amplitude is a little smaller than the experimental value. In addition, the maximum value of the in-line amplitude decreases with the increase of the damping ratio.

In general, the amplitude responses obtained by the model are basically consistent with the experimental results under different damping ratios, which further verify the correctness and extensiveness of the application of this model.

Similarly, the motion trajectories of the cylinder at $Ur = 6.5$ and 8.5 are given in Figure 12. It is found that the trajectory gradually changes from the '8' shape to the crescent shape with the increase of damping at $Ur = 6.5$, and the size of the trajectory has significantly decreased. This is because the Ur of the amplitude peak is smaller when the damping ratio is relatively large, which will result in the advanced appearance of the corresponding crescent-shape trajectory. When Ur is 8.5, the trajectory also changes with the damping ratio to the crescent shape, but variation of its size is relatively smaller. The reason for that is mainly the vibration starts to jump out of the lock-in region at $Ur = 8.5$, and the effect of the damping ratio on amplitude is relatively slighter.

4. Sensitivity analysis of the model parameters

In this paper, three types of empirical parameters are introduced, which are geometric nonlinear parameter η, coupling parameters h and ε as well as fluid oscillator damping parameters β and λ, respectively. In order to comprehensively analyse their effects on the prediction, an investigation of the sensitivity of above parameters has been performed.

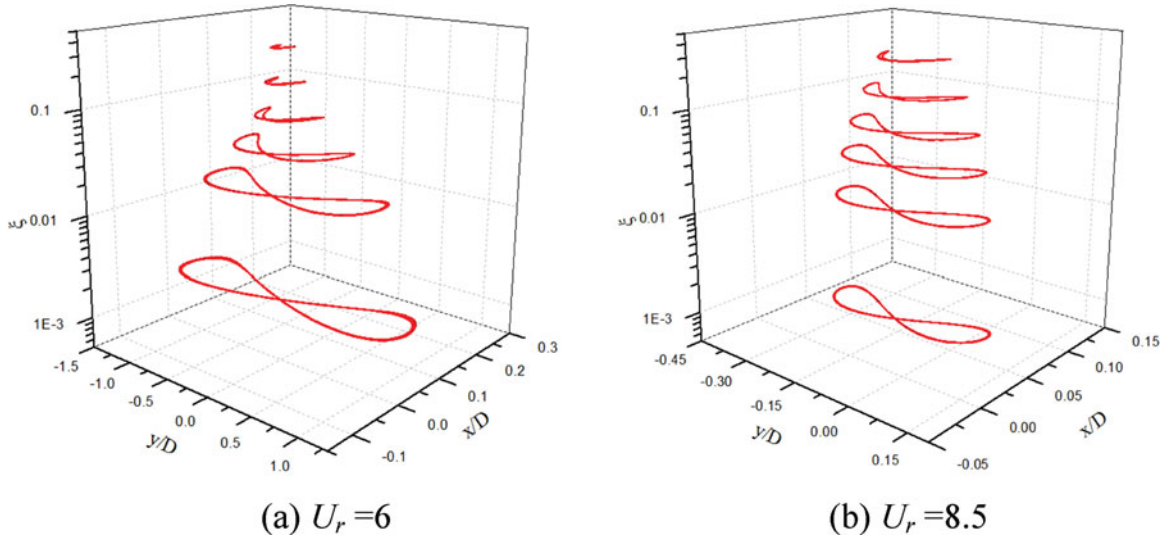

Figure 12. Comparison of the motion trajectories of the cylinders with different damping ratios; (a) $U_r = 6$; (b) $U_r = 8.5$. (This figure is available in colour online.)

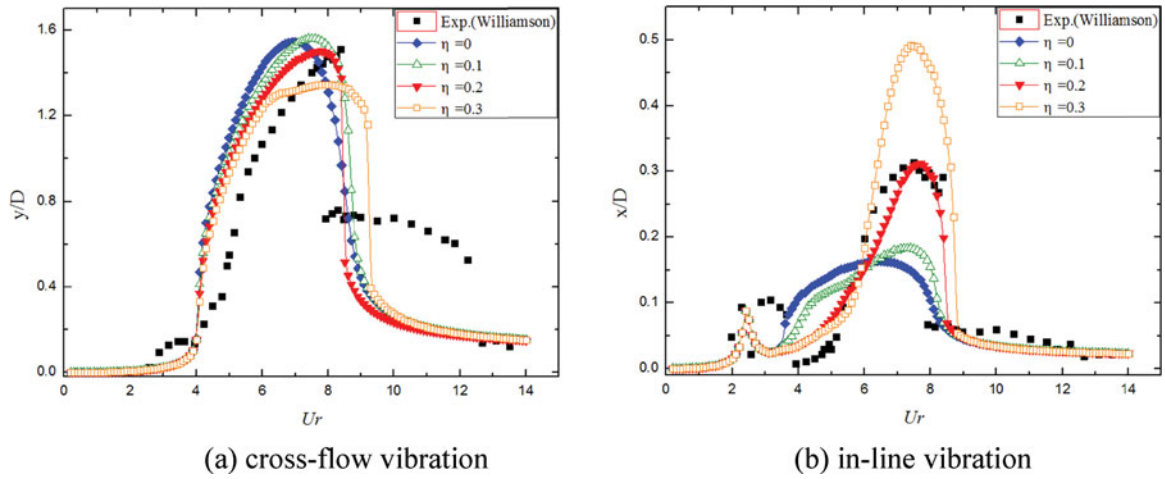

Figure 13. Comparison of the amplitude with different values of the geometric nonlinear parameter; (a) cross-flow vibration; (b) in-line vibration. (This figure is available in colour online.)

4.1. Analysis of the geometric nonlinear parameter

The geometrical nonlinear parameter η of the model is taken as 0, 0.1, 0.2 and 0.3, respectively in the calculation of the two-degree-of-freedom VIV of the cylinder. And by referring to the data of the model test about the two-degree-of-freedom VIV of a cylinder conducted by Jauvtis and Williamson (2004) in 2004, the mass ratio and damping ratio are selected as 2.6 and 0.005, respectively. And then, the predicting results are compared with Williamson's testing results, as shown in Figure 13.

It can be found that with the increase of parameter η, the cross-flow and in-line amplitude curves have changed obviously. For the cross-flow vibration, when η increases, the Ur corresponding to the peak of amplitude curve has an augment and the value of the peak also has a variation. And when η is 0.2, both the predicting maximum amplitude and the Ur corresponding to the peak of amplitude curve are close to the test results. For the in-line vibration, the shape of the amplitude curve changes with the η markedly. With the increase of η, the value of the second peak of in-line amplitude is also increasing, but the first peak value is basically consistent, which indicates the effect of η on in-line vibration mainly reflects in the coupled cross-flow and in-line item. And we can also find the results of in-line amplitude agree well with the test results at $\eta = 0.2$.

In general, as the value of η increases, the maximum cross-flow amplitude decreases while the maximum in-line amplitude increases, and the in-line amplitude response is more sensitive to η. And by analysing and selecting the value of the geometric nonlinear parameter, it is possible to realise the reasonable allocation of the coupling effect of cross-flow on in-line vibration.

4.2. Analysis of the coupling parameters

The coupling parameter ε is first analysed. Taking the test data of Stappenbelt et al. (2007) as a reference, we select the mass ratio and damping ratio as 5.19 and 0.006 and set the value of ε as 0.03, 0.066 and 0.1, respectively in the calculation. The comparison of the calculated and experimental results about the vibrating amplitude is shown in Figure 14.

It can be found that with the increase of parameter ε, the cross-flow and in-line maximum amplitudes are decreasing, and the width of lock-in interval also decreases slightly. For the cross-flow vibration, the Ur value corresponding to the peak decreases with the increase of ε. The difference between the

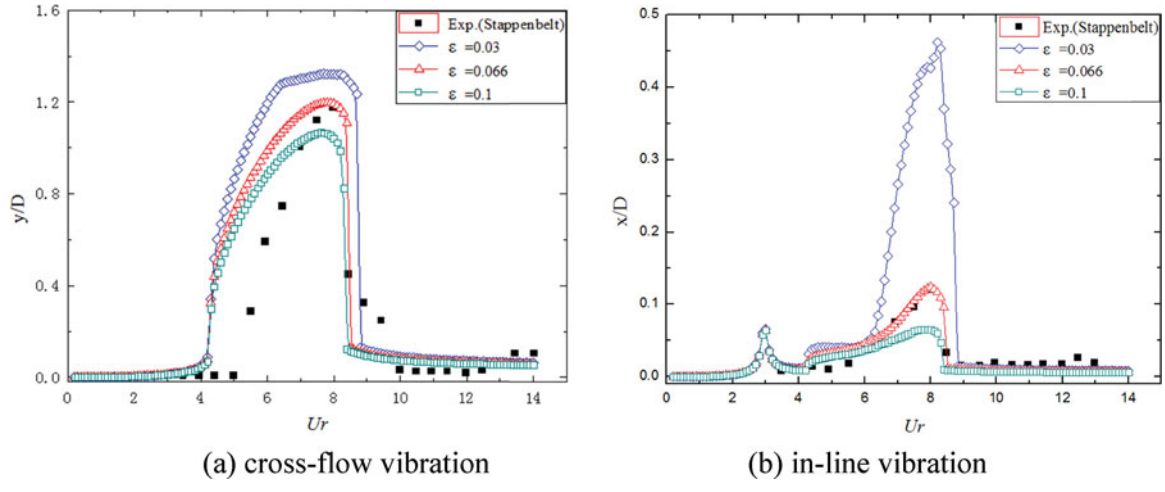

Figure 14. Comparison of the amplitude with different values of the parameter ε; (a) cross-flow vibration; (b) in-line vibration. (This figure is available in colour online.)

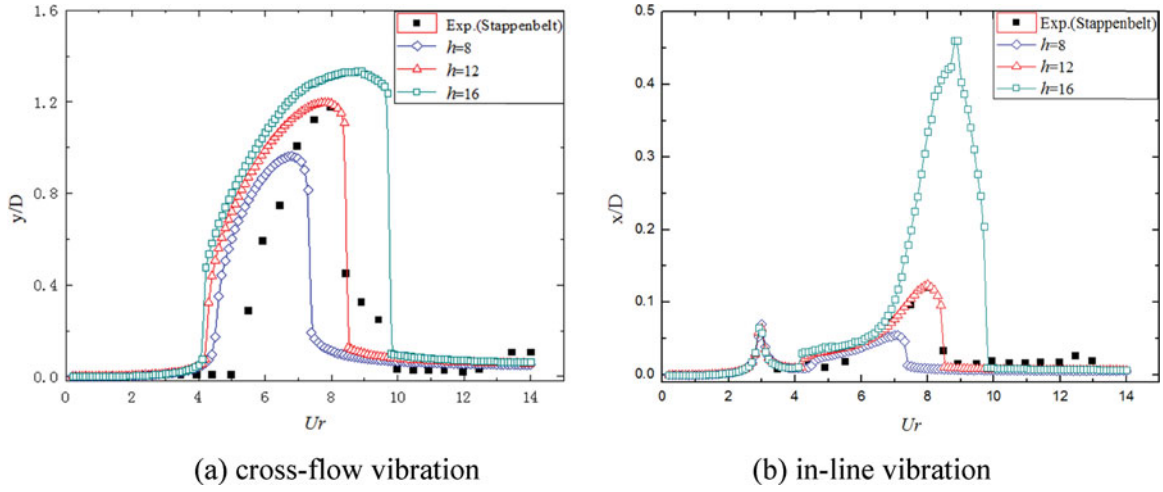

Figure 15. Comparison of the amplitude with different values of the parameter *h;* (a) cross-flow vibration; (b) in-line vibration. (This figure is available in colour online.)

three curves is mainly in the locked region, and when ε is 0.066, the model predicting results are in good agreement with the experimental results. For the in-line vibration, the shape of amplitude curve is more sensitive to the change of ε, and with the increase of ε, the coupling effect of cross-flow vibration on in-line vibration is becoming stronger, which makes the curve shape has a greater change. In summary, the role of ε is to adjust the value of cross-flow and in-line maximum amplitudes in the locked region.

For another coupling parameter h, we set it as 8, 12 and 16 in the prediction, respectively. The calculated results are compared with the test results obtained by Stappenbelt, as shown in Figure 15.

After analysis, it can be found that the parameter h not only has an effect on the value of the maximum amplitude, but also affects the width of the lock-in interval. As h increases, both the maximum amplitudes of cross-flow and in-line vibrations and the width of lock-in interval are increasing significantly. By contrast, the maximum amplitude, the width of lock-in interval and the shape of amplitude curve obtained by the mathematical model are in good agreement with the experimental results when h is 12, which is consistent with the research results of Facchinetti et al.

4.3. Analysis of the damping parameters of fluid oscillator

For the analysis of damping parameters β and λ, the mass ratio and damping ratio of the cylinder are still 5.19 and 0.006 in the calculation. According to the determination method for β and λ described in Section 2.4, the four groups of β and λ are selected and numbered as Schemes 1–4, respectively (see Table 2).

Considering β and λ may have a certain impact on the hysteresis interval, we have adopted the conditions of uniform acceleration and uniform deceleration, respectively in calculation. And then the calculated results of each scheme are compared with the experimental results, as shown in Figure 16.

By comparing and analysing the cross-flow amplitude curve, it can be found that the maximum amplitudes of the Schemes

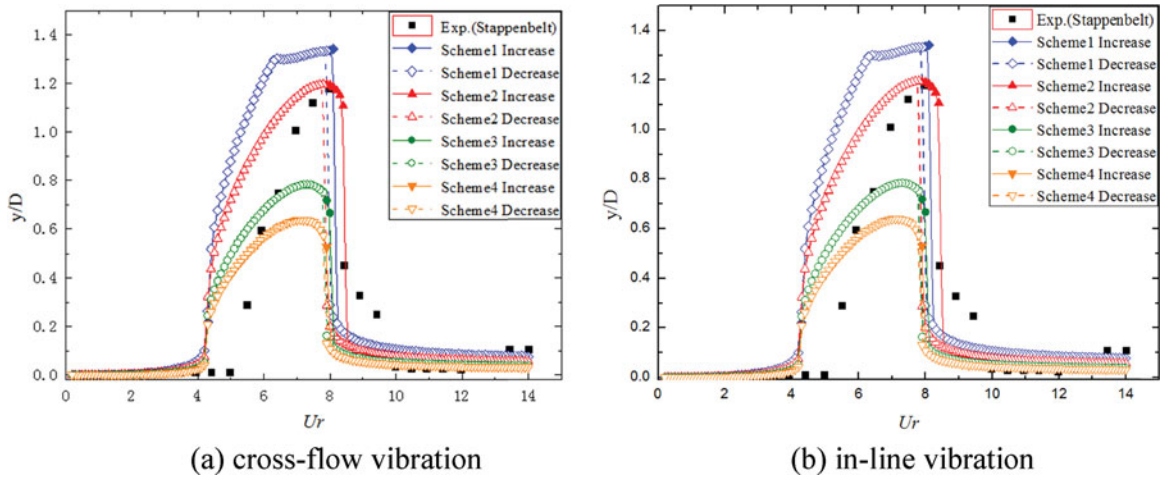

Figure 16. Comparison of the amplitude under different schemes of damping parameters; (a) cross-flow vibration; (b) in-line vibration. (This figure is available in colour online.)

Table 2. Selection schemes of the damping parameters.

Scheme number	β	λ
1	0.125	0.002
2	0.25	0.008
3	0.5	0.032
4	0.75	0.071

1–4 are decreasing, but the widths of lock-in interval and hysteresis interval are subjected to the process of increasing and decreasing, and the lock-in interval and the hysteresis interval of the Scheme 2 are the largest. Meanwhile, similar results have occurred in the in-line amplitude curve. And it is worth noting that the first peak of in-line amplitude curve has also changed, indicating that the value of the first peak is more sensitive to the variation of the damping parameters. So, the adjustment of the first peak can be achieved by reasonably changing the values of the fluid oscillator damping parameters. We can also find the result of Scheme 2 is better than that of other schemes, which indicates that the combination of the damping parameters determined in this paper is reasonable.

5. Conclusions

In this paper, by combining the nonlinear structural oscillator equation with the higher-order Van der Pol equation and deducing the fluctuating lift and drag based on the discrete point vortex theory, a higher-order nonlinear oscillator model which can predict the important characteristics of the two-degree-of-freedom VIV of a cylinder qualitatively and quantitatively has been proposed. Then, the model is verified in a classical cylinder example. And the vibrating characteristics under different mass ratio and damping ratio conditions are analysed. Finally, the sensitivity of the three types of parameters in the model is comprehensively studied. Through the above research, the following conclusions can be drawn:

(1) The vibrating amplitude and frequency under lower mass ratio condition calculated by the model proposed in this paper are in good agreement with the experimental results of Williamson, and the variation of the motion trajectory is consistent with the existing research, indicating that the model can predict the important characteristics of the VIV of the cylinder with lower mass ratio accurately. And the feasibility and reasonability of the application of the model are proved under the condition of lower mass ratio.

(2) The amplitude responses predicted by the model at different mass ratios and damping ratios are basically consistent with the experimental results conducted by Stappenbelt et al. And it is found that the mass ratio and damping ratio have a great influence on the cross-flow and in-line amplitude and trajectory in the calculation and model test. These results indicate that the higher-order nonlinear oscillator model can be used to predict the important characteristics of the two-degree-of-freedom VIV of cylindrical structures with different mass ratios and damping ratios, which verifies the universality of the application of the model.

(3) The sensitivity and effect of the geometric nonlinear parameter η, the coupling parameters ε and h as well as the fluid oscillator damping parameters β and λ are studied by using the control variable method. After comparison and analysis, it is found that η has an effect on both the cross-flow and in-line amplitude, and the value of amplitudes can be adjusted by selecting a reasonable η. The role of ε is mainly to adjust the peaks of cross-flow and in-line amplitude and the coupling effect between them. And the parameter h not only has an effect on the value of maximum amplitude, but also affects the width of lock-in interval. Besides, the value of the maximum amplitude, the parameters β and λ can also affect the size of hysteresis interval. In addition, by adopting the parameters selected in this paper, the amplitude characteristics of the VIVI can be accurately predicted, which indicates that the determination of the parameters in the model is reasonable and feasible.

In general, compared with the classical oscillator model, the higher-order nonlinear oscillator model has considered the nonlinear characteristics in two-degree-of-freedom VIV more fully and established the mathematical relationship between the fluctuating lift and drag, which can improve the accuracy of prediction effectively, especially for the 'super upper branch' of the amplitude response at lower mass ratio. And its range of application for mass ratio and damping ratio is more extensive. The model studied in this paper may provide some reference for the fast prediction of the VIV with two-degree-of-freedom for marine cylindrical structures.

Disclosure statement

No potential conflict of interest was reported by the authors.

Funding

This work was supported by the National Natural Science Foundation of China [grant number 51509046], [grant number 51509045], [grant number 51739001].

References

Bishop RED, Hassan AY. 1964. The lift and drag forces on a circular cylinder in a flowing fluid. R Soc London Proc. 277(1368):32–50.

Blevins RD, Coughran CS. 2009. Experimental investigation of vortex-induced vibration in one and two dimensions with variable mass, damping and Reynolds number. J Fluid Eng Trans ASME. 131(10):101202–101207.

Dolatabadi N, Farshidianfar A, Naranjani Y. 2011. Consideration of Lock-in using a modified wake oscillator in vortex induced vibrations about a cylinder. In: McIntyre Tim, editor. ISVA 2011. 1st International Conference on Acoustics and Vibration; Tehran, Iran. p. 1272.

Facchinetti ML, Langre ED, Biolley F. 2002. Vortex shedding modeling using diffusive Van der Pol oscillators. Comptes rendus – Mécanique. 330(7):451–456.

Facchinetti ML, Langre ED, Biolley F. 2004. Coupling of structure and wake oscillators in vortex-induced vibrations. J Fluid Struct. 19(2):123–140.

Farshidianfar A, Zanganeh H. 2010. A modified wake oscillator model for vortex-induced vibration of circular cylinders for a wide range of mass-damping ratio. J Fluid Struct. 26(3):430–441.

Gao Y, Zong Z, Zou L, et al. 2017. Effect of surface roughness on vortex-induced vibration response of a circular cylinder. Ships Offshore Struct. 13(1):28–42.

Govardhan R, Williamson CHK. 2000. Modes of vortex formation and frequency response of a freely vibrating cylinder. J Fluid Mech. 420:85–130.
Griffin OM, Skop RA. 1976. The vortex-induced oscillations of structures. J Sound Vib. 44(2):303–305.
Guilmineau E, Queutey P. 2004. Numerical simulation of vortex-induced vibration of a circular cylinder with low mass-damping in a turbulent flow. J Fluids Struct. 19(4):449–466.
Hartlen RT, Currie IG. 1970. Lift-oscillator model of vortex induced vibration. J Eng Mech. 96(5):577–591.
Hartlen RT, Currie IG, Hartlen RT, Currie IG. 1970. Lift-oscillator model of vortex-induced vibration. J Eng Mech Div. 96(5):577–591.
Jauvtis N, Williamson CHK. 2004. The effect of two degrees of freedom on vortex-induced vibration at low mass and damping[J]. J Fluid Mech. 509:23–62.
Landl R. 1975. A mathematical model for vortex-excited vibrations of bluff bodies. J Sound Vib. 42(2):219–234.
Nayfeh, AH. 1979. Introduction to perturbation techniques. New York (NY): Wiley.
Nguyen VT, Nguyen HH. 2016. Detached eddy simulations of flow induced vibrations of circular cylinders at high Reynolds numbers. J Fluids Struct. 63:103–119.
Ogink RHM, Metrikine AV. 2010. A wake oscillator with frequency dependent coupling for the modeling of vortex-induced vibration. J Sound Vib. 329(26):5452–5473.
Pantazopoulos MS. 1994. Vortex-induced vibration parameters: Critical review. In: Proceedings of the 17th International Conference on Offshore Mechanics and Arctic Engineering; Osaka, Japan. pp. 199–255.
Prasanth TK, Mittal S. 2008. Effect of blockage on free vibration of a circular cylinder at low Re. Int J Numer Methods Fluid. 58(10): 1063–1080.
Qin W, Kang Z, Song R. 2012. Research on wake-oscillator model in 2-DOF vortex-induced vibration of cylinder based on discrete point vortex. Eng Mech. 29(9):294–299.
Rahman MAA, Leggoe J, Thiagarajan K, Mohd MH, Paik JK. 2016. Numerical simulations of vortex-induced vibrations on vertical cylindrical structure with different aspect ratios. Ships Offshore Struct. 11(4):1–19.
Srinil N, Zanganeh H. 2012. Modeling of coupled cross-flow/in-line vortex-induced vibration using double duffing and Van der Pol oscillators. Ocean Eng. 53(3):83–97.
Stappenbelt B, Lalji F, Tan G. 2007. Low mass ratio vortex-induced motion. In: Jacobs P, editor. AFMC 2007. Proceedings of the 16th Australasian Fluid Mechanics Conference Crown Plaza, Gold Coast; Queensland, Australia. p. 201–209.
Wanderley JBV, Soares LFN. 2015. Vortex-induced vibration on a two-dimensional circular cylinder with low Reynolds number and low mass-damping parameter. Ocean Eng. 97:156–164.
Xu J, Wang D, Huang H, Duan M, Gu J, An C. 2017. A vortex-induced vibration model for the fatigue analysis of a marine drilling riser. Ships Offshore Struct. 12(Sup1):S280–S287.
Zdravkovich MM. 1985. Flow induced oscillations of two Interfering circular cylinders. J Sound Vib. 101(4):511–521.
Zhu H, Gao Y. 2017. Effect of gap on the vortex-induced vibration suppression of a circular cylinder using two rotating rods. Ships Offshore Struct. 13(2):1–13.